Stanford Mathematical Geophysics Summer School Lectures

Basics of Exploration Seismology and Tomography

Gerard T. Schuster
Geology and Geophysics Department
University of Utah

Preface

"Do not use more mathematics than the data deserve" paraphrase from Sven Treitel

This series of lectures notes is aimed at quickly introducing mathematicians to some aspects of exploration seismology. I tried to avoid algebraic complexity and presented only the key ideas. The HTML lectures and MPG movies associated with the lectures are online at *http://utam.gg.utah.edu/stanford/stanford.html*. A Netscape 4.0 or higher browser is recommended.

The first lecture, *Basics of Seismic Experiments and Data Processing*, provides a quick look at seismic experiments, data processing, and the final product, the seismic section. The central idea behind each processing step is explained with a minimal use of algebra. I have used many data processing examples to explain the processing steps, and MATLAB scripts are used to clarify any ambiguities in the procedures. The one processing step not described is Dip Moveout Processing, which is not necessary when prestack migration is used. It is my hope that the first lecture can provide sufficient background information so that the mathematician can appreciate the exploration context for the more sophisticated ideas presented by other lecturers. After the first formal lecture, we will conduct a seismic experiment outside the classroom and analyze the data.

The second lecture on *Basics of Traveltime Tomography* describes the theory behind inversion of traveltime data and presents some interesting examples. As before, the central ideas are presented but the mathematical details are kept to a minimum. Examples are given for both exploration and earthquake seismology.

The third lecture presents the *Basics of Waveform Tomography*. I present the theory, followed by a discussion on the benefits and pitfalls of waveform tomography. By no means is this a comprehensive treatment, but it can serve as the starting point for further exploration.

Jerry Schuster (schuster@mines.utah.edu)
Geology and Geophysics Department
University of Utah

Contents

Basics of Exploration Seismic Experiments and Data Processing

---

Introduction

The goal of exploration seismology is to find oil and gas reservoirs by seismically imaging the earth's reflectivity distribution. Towards this goal, exploration geophysicists perform seismic experiments ideally equivalent to that shown in Figure 1. Here, the source excites seismic waves, and the resulting primary reflections are recorded by a geophone located at the source position. If we assume only primary reflections then this defines the ideal zero-offset (ZO) experiment. For now we assume a magic filter (to be described later as data processing) that eliminates all events but primary reflections.

A seismic source is usually some mechanical device or explosive that thumps the earth, and a geophone records the time history of the earth's vertical particle velocity, denoted as a seismic trace $d(x,z=0,t)$. Larger amplitudes on the Figure 1 traces correspond to faster ground motion and the up-going (down-going) motion is denoted here by the blackened (unblackened) lobes. The strength of these amplitudes is roughly proportional to the reflectivity strength $m(x,z)$ of the corresponding reflector. Assuming a constant density and a 1-D medium , the reflectivity $m(x,z)$ is roughly defined as as

$$m(x,z) \quad \cong \quad \frac{v(z+dz)-v(z)}{v(z+dz)+v(z)}, \tag{1.1}$$

where $v(z)$ is the propagation velocity at depth z.

After recording at one location, the source and receiver are moved a bit over and the idealized ZO seismic experiment is iteratively repeated for different ground positions. All recorded traces are lined up next to one another and the resulting section is defined as a ZO or poststack seismic section, as shown on the RHS of Figures 1 and 2. Note that the depth d of the first reflector can be calculated by multiplying the 2-way reflection time t by half the velocity v of the first layer, i.e. $d = tv/2$.

The reflection section in Figure 1 roughly resembles the actual geology, where one side of the signal is colored black to help enhance visual detection of the interface. Unfortunately, this experiment and the ZO seismic section are ideal because they assume no coherent noises such as multiples, out-of-the-plane scattering, surface waves, converted waves and so on. In practice, a real ZO experiment cannot generate the ideal seismic section because the source also generates strong coherent noise and near-source scattering energy. To solve this problem, explorationists perform non-zero offset experiments (where one shot shots into many far-offset geophones), filter coherent noise from these data and make time-shift corrections to the traces so that they are roughly equivalent to the ideal ZO traces. The steps for processing these data are described in a later section.

Figure 1.1: Figure 1. Earth model on left and idealized zero-offset (ZO) seismic section on right, where each trace was recorded by an experiment where the source has zero offset from the geophone. The above ZO seismic section represented by d(x,z=0,t) roughly resembles the earth's reflectivity model m(x,z) because we unrealistically assume it contains only the primary reflections.

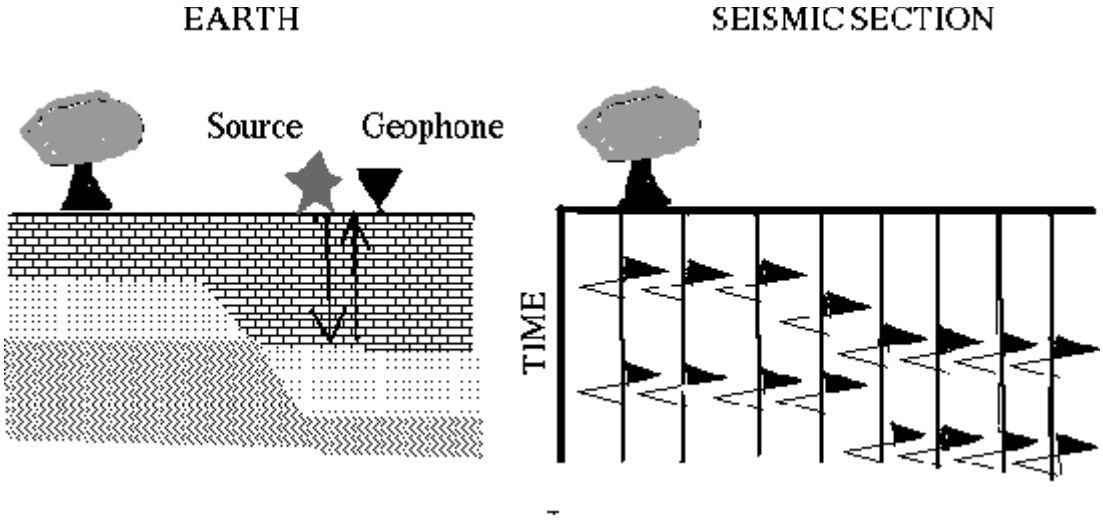

Seismic Experiment

In practice the ZO shooting geometry shown in Figure 1 does not produce useful results because the signal/noise (S/N) ratio is too low. This is in part due to the very weak zero-offset reflections , strong coherent noise, and strong scattering (?) noise near the source. To suppress these noises, the seismic reflection experiment is designed to record arrivals that are offset from the source position, as shown in Figure 1.5. This figure shows a 2-D recording geometry where the source shoots into a 1-D recording line of receivers or geophones, and the resulting reflections are recorded by the recording truck. This is referred to as a 2-D recording line because the reflections are assumed to emanate only along the vertical XZ plane coincident with the recording line. The length of the recording line is sometimes referred to as a cable length.

Figure 1.5: Typical shooting geometry for a 2-D end-line seismic experiment, where the shot is at one end of the spread. After excitation of the shot, the stations and shot are moved by the same amount and the experiment is iteratively repeated.

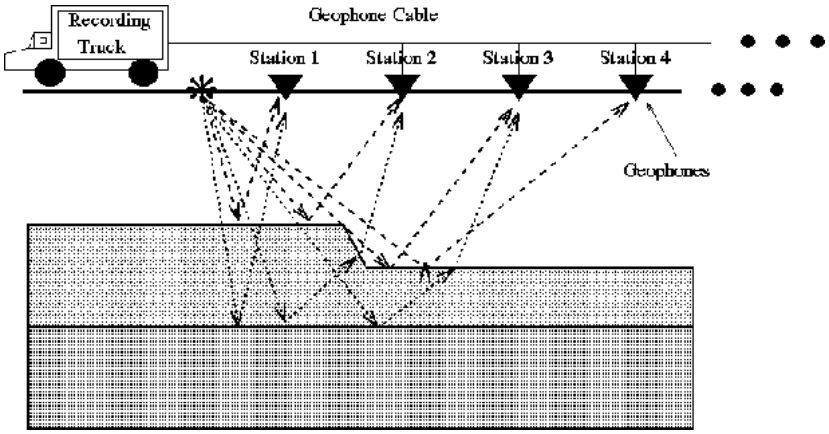

Seismic Sources

There are many types of seismic sources, but the most often used sources for land surveys are vibrator trucks (see Figure 1.6), and for marine surveys are air guns. Vibrator trucks continuously shake the ground, starting from a low frequency rumble at about 5 Hz and then progressively sweep to higher frequencies up to 150 Hz. The sweep time

ranges from 20 s to 40 secs or so, and the recorded signal is crosscorrelated with the vibrator truck signal to produce an impulsive source wavelet.

Figure 1.6: Typical land and marine sources. Vibroseis truck above is workhorse of land surveys, where truck lifts up on center pad and vibrates up and down for about 20-40 secs per station. Sometimes 5 or more trucks vibrate simultaneously, and are evenly spread out over an interval equal to the wavelength of a surface wave so that the groundroll is canceled by destructive interference. Air guns are the preferred source for marine surveys, and muscle power is the preferred cost-effective source for U of Utah surveys at the bottom.

Recording Equipment

Typical exploration surveys lines record from 48 to over 1000 channels of data per shot, where there might be anywhere from 50 feet to over 300 feet between takeouts or geophone stations. To avoid spatial undersampling or aliasing, the shot intervals and the takeout distances are usually no more than 1/2 the wavelength of your important

reflection events. However, economic considerations prevent this ideal shot or receiver interval from being fully realized in most 3-D surveys. See Figure 1.7 for views of the recording box, geophones and the source used in a recent Moab, Utah experiment that searched for clues to a large meteorite impact.

To increase the signal-to-noise, at any one takeout station there may be many geophones (from 6 to over 48 in a group) connected in series to one another so that the summed signal is linked to one channel in the multi-channel recording cable. Similarly, there may be several sources spaced out so as to cancel the surface waves or ground roll (see top right picture in Figure 1.6). If the *group length* (i.e., maximum separation between any two geophones in a group) is about the same as the wavelength of the surface wave, then the serial geophones in a group tend to cancel the short wavelength surface waves while passing the long wavelength reflected waves.

Figure 1.7: Clockwise starting from top left: Receiver cables and geophones, cable spool, weight drop source, and 48-channel portable Bison recorder in Moab, Utah experiment.

Common Shot Point Gathers

The traces recorded by a single shot are grouped together to form a *common shot gather or CSG*, as shown on the LHS of Figure 1.8. Note that the R2 reflection times increase with an increase of source-receiver offset, and these reflections are readily identified for source-receiver offsets greater than 60 feet. Near the zero-offset locations these reflections are buried by near-source noise.

Figure 1.8: Common shot gather on left and skeletonized version depicting arrival traveltimes vs X for the direct (D), Refracted (Ref1) and Reflected (R2) arrivals. The apparent velocities dx/dt of these arrivals can be measured from the x-t graph. CSG data collected along W. Valley Fault, Utah,

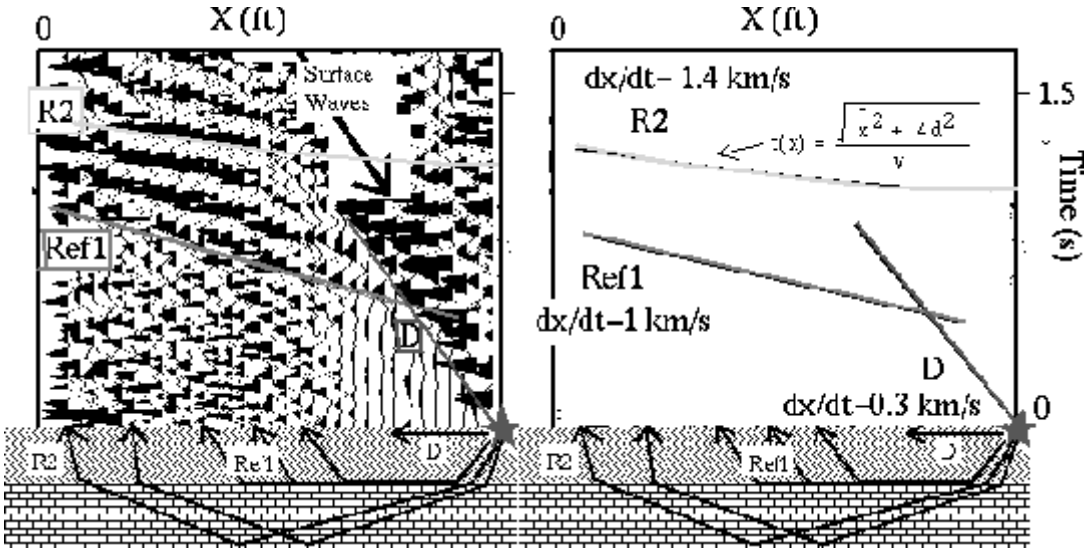

To cover a greater subsurface area with reflection events, the shot and geophone locations are translated (or *rolled along*) by the same distance and the CSG experiment is repeated to give another shot gather. These experiments are repeated along a line until sufficient subsurface coverage has been achieved. Play the *html* movie to see how CSG's are collected and the correspondence between traces and raypaths. It is usually necessary to have a long recording line so that 1). the noise near the source is avoided, 2). the surface wave amplitude has diminished or the slow surface waves arrive much later than the reflections, 3). the moveout trajectory of the reflection events is sufficiently distinguished from coherent noise trajectories so that processing (i.e., stacking) removes the noise, and 4). there is better spatial resolution in the seismic image. The seismic camera is similar to an optical camera, where wider apertures result in better image resolution.

In Figure 1.8, the non-zero offset reflections arrive later than the ideal zero-offset reflection. Therefore, to realize the goal of obtaining an ideal ZO section we must apply time shifts to the non-zero offset reflections to correct them to zero-offset time. To do this we must reorganize the data into a *common midpoint gather* (*CMG*) as explained in the next section.

Common Midpoint Gathers

The CSG data are reorganized so that they are in the form of common midpoint gathers, where any trace in a CMG has the same source-receiver midpoint as any other trace in the CMG.

A CMG collected along the Oquirrh Fault, Utah is shown in Figure 1.9. Here the midpoint x_m and half-offset x_h coordinates in a CMG are related to the source x_s and geophone x_g coordinates in a CSG by

$$x_m = (x_g + x_s)/2 \quad ; \quad x_h = (x_g - x_s)/2 \; . \tag{1.2}$$

The beauty of the CMG is that each trace contains reflection energy that sampled the same part of the reflector as the other traces in the CMG. As an example, the R3 reflection events along the R3 hyperbola in Figure ❑ all emanated from apex of deepest raypath shown in this figure. This redundancy will be exploited (as discussed later) by stacking these redundant reflections together to increase the S/N ratio of the seismic record. In contrast, the R2 reflections in the CSG in Figure 1.8 emanate from different parts of this reflector and so do not redundantly sample the R2 reflector.

Figure 1.9: Similar to previous figure, except 1). traces in CSG's are reorganized into a CMG, and 2). the above data were collected along Oquirrh Fault, Utah. Note, each ray shown above is connected with a source-receiver pair, and all such pairs share the common midpoint location denoted by the filled square box. The thick hyperbolic lines describe the moveout curves for primary reflections.

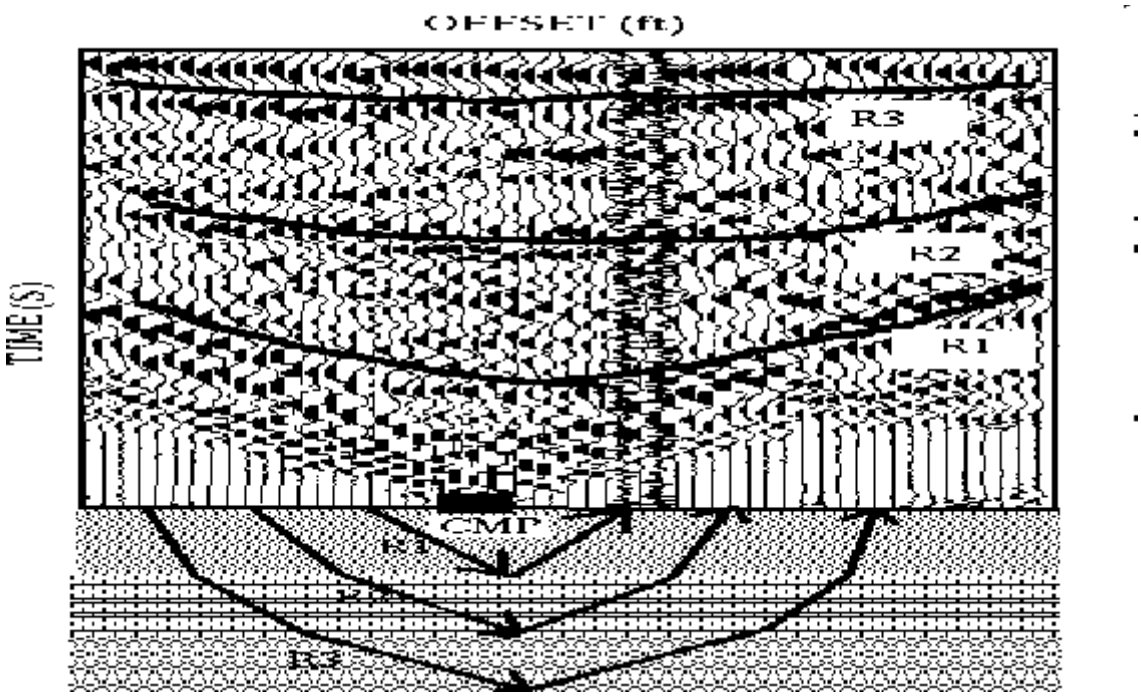

Figure 1.10 depicts the rays and traces associated with CSG's and CMG's, and the *html* movie shows how these data were created. Note, all of the common midpoint (CMP) rays in the second to the bottom graph in Figure 1.10 emanate from the same reflection point.

The number of traces in a CMP gather defines the *fold*of the data. For example, the total number of traces in Figure 1.9 define the fold number. Large fold data means we have redundantly sampled a subsurface reflection point many times, so that after stacking (explained below) we will most likely have a stacked trace with a good S/N ratio. From the *html* movie, note the fold of a CMG decreases as the midpoint position approaches the end of the recording aperture.

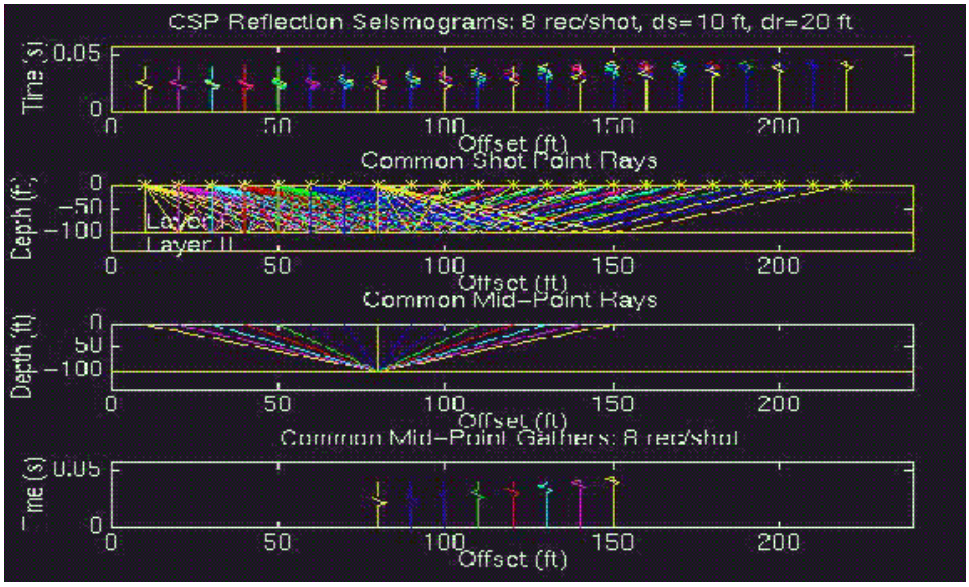

The next step in order to realize the goal of ideal ZO data is to apply time shifts (i.e., Normal Moveout (NMO) corrections to be discussed in the next section) to the traces in a CMP gather to correct them to the zero-offset reflection time. These corrected traces in the CMG are then added together (i.e., stacked) to produce a stacked trace with a large S/N ratio. Presumably, most of the coherent noise can be eliminated by this stacking process because the time shifts only aligned the reflections with one another so that only the primary reflections coherently added together after stacking.

Apparent Velocity

We are almost ready to begin processing the CSG data to achieve the goal of obtaining the ideal ZO section. But first we explain the useful idea of an event's moveout velocity. A moveout velocity can be used to distinguish reflection events from coherent noise such as surface waves or multiples.

Figure 1.9 depicts arrivals that *moveout* from the source position with offset. The *apparent velocity* v_x in the x direction of an arrival can be computed by measuring the slope $v_x=dx/dt$ of that event's arrival time curve $t(x)$, as shown on the RHS of Figure 1.8. Arrivals with a large apparent velocity and having a hyperbolic moveout curve are usually reflection events. For example, a 2-layer flat medium with a first layer velocity of v and an interface depth of d would see the traveltime equation for the primary reflections as

$$t(x) = \sqrt{4d^2 + x^2}/v = \sqrt{t(0)^2 + x^2/v^2} \qquad (1.3)$$

where $t(0)=2d/v$ is the 2-way vertical traveltime to the reflector at depth d. This equation describes a hyperbolic curve and characterizes the hyperbolic trajectory of reflection events seen in Figure 1.8 or 1.9.

Check out the *html* movie to see how plane waves propagate with different apparent velocities for different incidence angles.

RMS Velocity

If the homogeneous medium is replaced by a stack of horizontal layers then the traveltime equation can be replaced by a series expansion in the offset coordinate:

$$t^2(x) = C_0+C_1x^2+C_2x^4+\ldots \ , \qquad (1.4)$$

where $C_0=t(0)^2$, $C_1=1/v_{RMSN}^2$, and the other coefficients are complicated terms. Here, the *RMS* velocity v_{RMSN} for the stack of N layers is defined by

$$v_{RMSN}^2 \cong \frac{\sum_i^N v_i^2 \Delta t_i}{\sum_{i=1}^N \Delta t_i}, \qquad (1.5)$$

where Δt_i is the vertical 2-way time through the *ith* layer, and $t(0)$ in equation 1.3 becomes

$$\sum_{k=1}^N \Delta t_i$$

equal to the 2-way vertical traveltime to the *Nth* layer. Note that v_{RMSN} depends on the the number of layers N, so we say that the *Nth* reflector has a different v_{RMSN} value than, say, the N-4 reflector.

Plugging equation 1.5 into 1.4 and truncating after 2 terms yields the traveltime equation for short offsets and a multilayered media:

$$t(x) = \sqrt{t(0)^2 + x^2/v_{RMS_N}^2}. \qquad (1.6)$$

The approximation in the above equation is valid for small values of offset x (Yilmaz, 1987). Once the v_{RMSN} velocity is found for each reflector then the interval velocities v_n can be found by the Dix formula:

$$V_n^2 = \frac{v_{RMS_n}^2 t(0)_n - v_{RMS_{n-1}}^2 t(0)_{n-1}}{t(0)_n - t(0)_{n-1}}, \qquad (1.7)$$

where $t(0)_n$ denotes the vertical reflection traveltime to the *nth* layer. The validity of this formula is easily proven by using the definition of $v_{RMSN}$and simple algebraic manipulation.

In summary we have learned some new words.

1. STATION: Recording site connected to a group of geophones. Data from this site is transmitted along one channel in recording line.
2. GEOPHONE Group: Geophones serially connected, and summed signal is fed to one channel.
3. SPREAD LENGTH: Length of recording line.
4. ZO SECTION: Seismic traces obtained by recording seismic energy with a geophone that has zero offset from the source.
5. CSG: Common shot gather of traces recorded with a common shot.
6. CMG: Common midpoint gather of traces where each of the traces have the same midpoint position between the shot and receiver.
7. SHOT AND GROUP INTERVALS: Intervals between shot points and stations.
8. APPARENT VELOCITY: Velocity of an arrival as measured along a horizontal line.
9. ENDLINE AND MIDPOINT RECORDING GEOMETRIES: Shot at end of recording line = endline. Shot at midpoint of recording line = midpoint.
10. The fold number is the number of traces in a CMG. It is the number of traces in a gather with a common reflection point.

Basic Processing Steps

Some basic processing steps are needed to obtain ZO sections from CSG's.

1- Automatic Gain Control to Correct for Geometrical Spreading+Anelastic Losses.

The seismic amplitudes are usually strongest nearest the source and at early times. Consequently, the raw records usually show very weak or non-existent reflections at the far-offset traces. To display these important signals we gain the data in some fashion. This gain procedure can be a combination of several methods:

- Backing out the geometric spreading by multiplying each trace with the reciprocal of the geometric spreading factor $v(t)*t$, where $v(t)$ is velocity at time $t$and t is the 2-way traveltime. The attenuation can also be backed out by multiplying the trace with $e^{|\alpha|t}$, where $\alpha$is the attenuation constant.
- Automatic gain control (AGC) of the data. Here the data within a specified time window is gained to a constant energy level. The window is slid down the trace so the energy is equilibrated. Shorter windows boost everything while longer windows tend to show true relative amplitudes.

```
%
% MATLAB 5.0 script for applying AGC to CSG traces in a CSG.
% For each trace, the energy within a moving window of length
% np is computed and the sample in the center part of this window
% is divided by this energy.
%
% data(x,t)    - input - nx x nt CSG matrix
% np           - input - length of AGC window
% out1         - output- traces with AGC applied
%
[nx,nt]=size(data);
inn=[fliplr(data(:,1:np)) data fliplr(data(:,nt-np:nt))];
inn=inn.^2;
f=ones(np,1)/np;
out=conv2(inn,f');
start=round(np+np/2);endd=start+nt-1;
outt=out(:,start:endd);
out1=data./(sqrt(outt)+.000001);
```

2- Muting.

We use a brute force mute to eliminate events that are not coincident with our beloved primary reflections, e.g., surface waves that arrive earlier than reflections. Figure 1.11 depicts a shot gather before (LHS CSG) and after 50-280 Hz bandpass filtering (RHS image).

Figure 1.11: CSG seismograms before (LHS) and after (RHS) muting of data before first arrival.

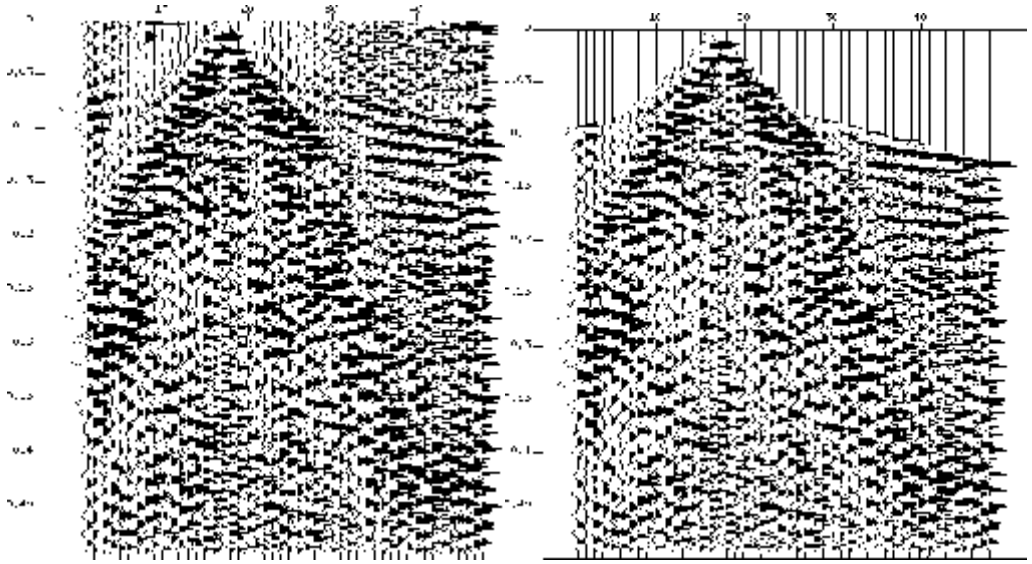

3- Bandpass Filter Data to Remove Noise.

If the noise and signal are separated in the temporal frequency domain, then bandpass filtering can applied to the traces to remove such noise. Strong noise might be low-frequency surface waves, 60 Hz electrical noise, wind noise, mechanical noise from human environment, cows or sharks munching on cables, etc..

As an example, Figure 1.12 depicts a shot gather before (LHS CSG) and after 50-280 Hz bandpass filtering (RHS image). Much of the low frequency groundroll (i.e., surface waves) has been eliminated to reveal many reflection events with pseudo-hyperbolic trajectories.

Figure 1.12: CSG seismograms before (LHS) and after (RHS) 50-280 Hz bandpass filtering. The low frequency surface waves have been suppressed.

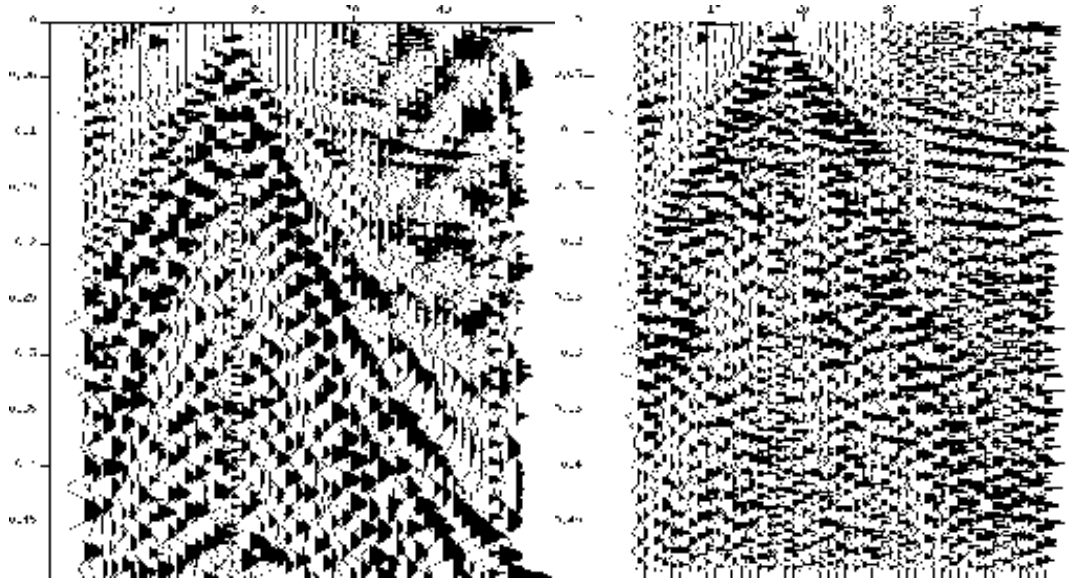

4- Static Corrections to Remove Elevation and Near-Surface Heterogeneities.

A major goal of reflection processing is to provide reflectivity images of the correct reflector geometry. This goal can be thwarted by the statics problem. The statics problem is defined to be static time shifts introduced into the traces by, e.g., near-surface velocity anomalies and/or topography. These time shifts distort the true geometry of deep reflectors.

As shown in Figure 1.13, an undulating topography can produce moveout delays in the CSG that can also be interpreted as undulations in the reflector, even if the reflector is flat. After an elevation statics correction (i.e., time shifts applied to traces) the data appear to have been collected on a flat datum plane. Figure 1.13 shows that static shifts can also be introduced by near-surface velocity anomalies which usually delay the traveltimes, resulting in reflections having a non-hyperbolic moveout curve.

Static shifts introduced by topographic variations fall under the class of field statics, and those due to near-surface lithological variations that occur within a cable length fall under the class of *residual statics*. Correcting for static shifts in the traces can make a significant difference in the quality of a migrated or stacked image. It is easy to determine elevation static corrections, but not so easy to find the residual static corrections. One means is to determine the near-surface velocity distribution by refraction tomography, which will be discussed later.

Figure 1.13: (LHS) Elevation static correction applied to CSG traces to correct data so that it appears to have been shot on a level datum plane. Still, there is a residual static correction which must be removed to correct for the low-velocity pod.

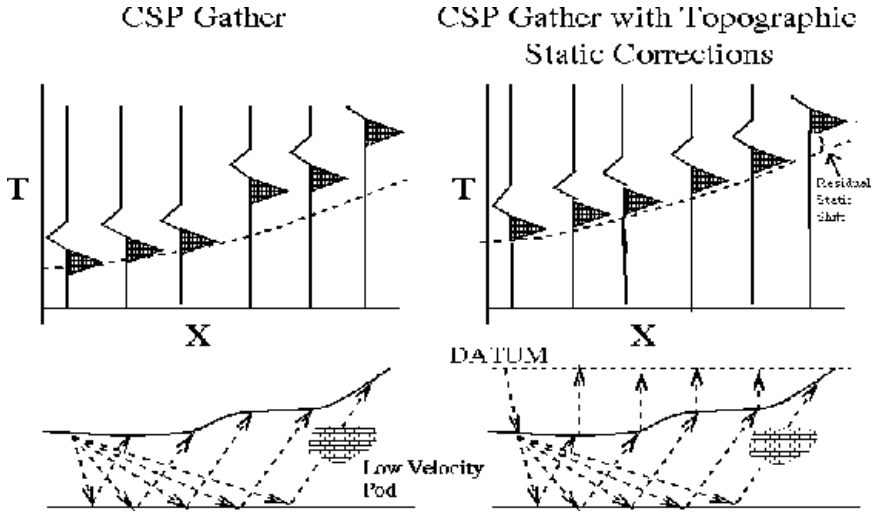

Figure 1.14: CMG collected over the Oquirrh fault, Utah where the jitter in the reflections at depth is due to near-surface velocity variations. These jitters must be corrected prior to NMO correction and stack.

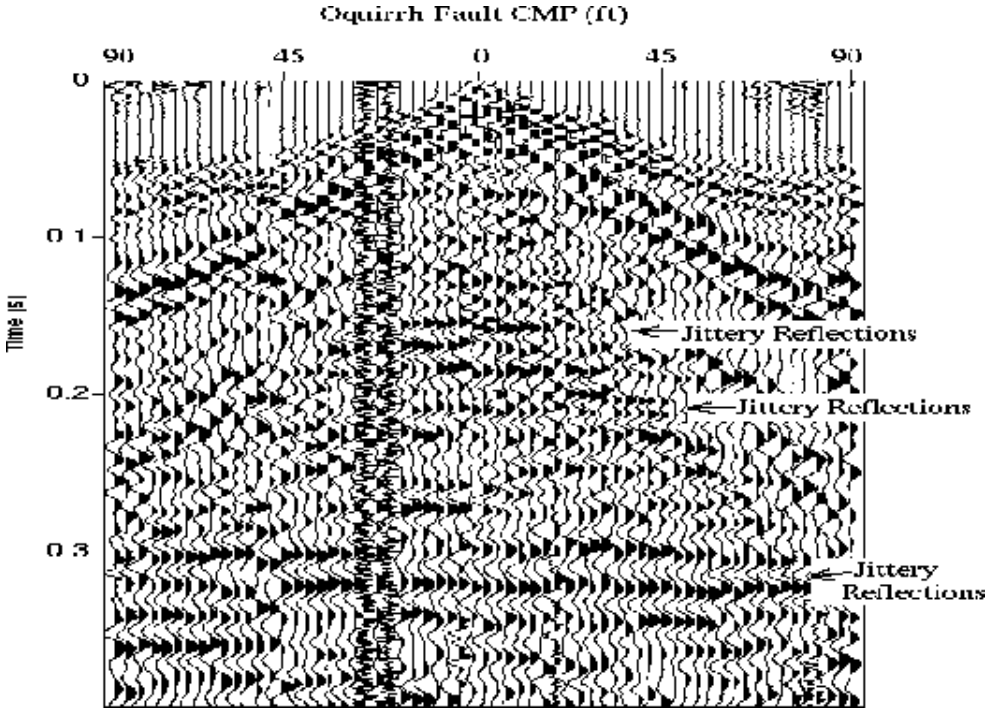

5- Velocity Filter Data to Remove Surface Wave Noise.

Events with a slow moveout velocity (1000-4000 ft/s) are typically unwanted noise such as surface waves. Their velocity is usually well separated from the apparent velocity of deep reflections so we can filter them out in a domain in which they are well separated from one another, namely the FK (i.e., frequency-wavenumber) domain.

As an example, assume the data $d(x,t)$

$$d(x,t) = \delta(x - v_{slow}t + x_0) + \delta(x - v_{fast}t + x_0'), \tag{1.8}$$

consist of two linear events, one moving out with a slow velocity v_{slow} and the other with a fast velocity v_{fast}. The x-intercepts are denoted by x_0 and x_0'.

In the (x,t) domain the two linear events cross one another and so it is difficult to mute one entirely from the other. However, under an FK Fourier transform the above equation becomes:

$$\tilde{d}(k,\omega) = a\delta(kv_{slow} - \omega) + b\delta(kv_{fast} - \omega), \tag{1.9}$$

where a and b are phase terms. It is clear the transformed data describe two slanted lines that do not cross each other except at the origin. Thus muting one line from the other based on their different slopes (i.e., velocities) is trivial in the FK domain.

The above procedure is called velocity filtering. As a field data example, Figure 1.15 shows a CSG before and after velocity filtering to remove the steep surface waves.

Figure 1.15: CSG seismograms before (LHS) and after (RHS) FK velocity filtering to eliminate surface waves.

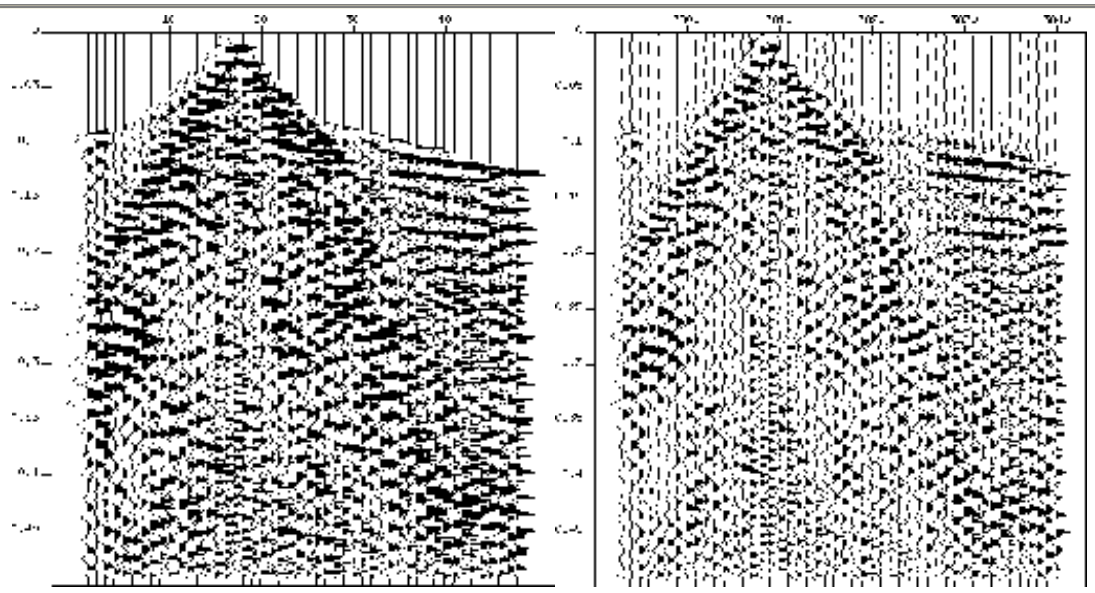

6- Normal Moveout Correction to Align Offset Reflections with ZO Reflections.

The CMG traces in Figure 1.9 are misaligned with one another so that a brute stack will produce cancellation of the signal. To avoid this cancellation we flatten out the reflections by using equation 1.6 to apply a normal moveout (NMO) time shift $t_{NMO}(x)$ to the data, where

$$t_{NMO}(x) = t(x)-t(0),$$

$$= t(0)[\sqrt{1+(x/v_{NMO}t(0))^2}-1], \qquad (1.10)$$

and we have replaced the v_{RMS} by v_{NMO}. Once flattened, the traces in a NMO-corrected gather can be stacked together for constructive reinforcement of the reflection events.

But how do we in practice determine the v_{NMO} values? A systematic means for determining Vnmo is described in the next section on velocity analysis.

The MATLAB script for NMO corrected data is given below:

```
%
% data(x,t)     = CMG data
% datanmo(x,t)  = CMG data with NMO correction
% t0            = 2-way normal incidence time
% v(t0)         = Stacking velocity as a function of 2-way normal incidence time
%
for x=1:nx;
for t0=1:nt;
 tx = sqrt(t0^2+(x*2/v(t0))^2);
 datanmo(x,t0) = data(x,tx);
end;
end;
```

Application of a script like this to the LHS of Figure 1.16 will "flatten" the primary reflections to give the NMO corrected traces shown on the RHS.

Figure 1.16: Mobil's Gulf of Mexico CMG (LHS) before and (RHS) after NMO correction. Note, the absence of surface waves (why?) and the cleaner appearance (no static problems) of these marine records compared to the messy land data from Utah. Marine data, typically, are cheaper to acquire and cleaner than land data. The primary problem with marine data, however, is usually the presence of sea-floor multiples.

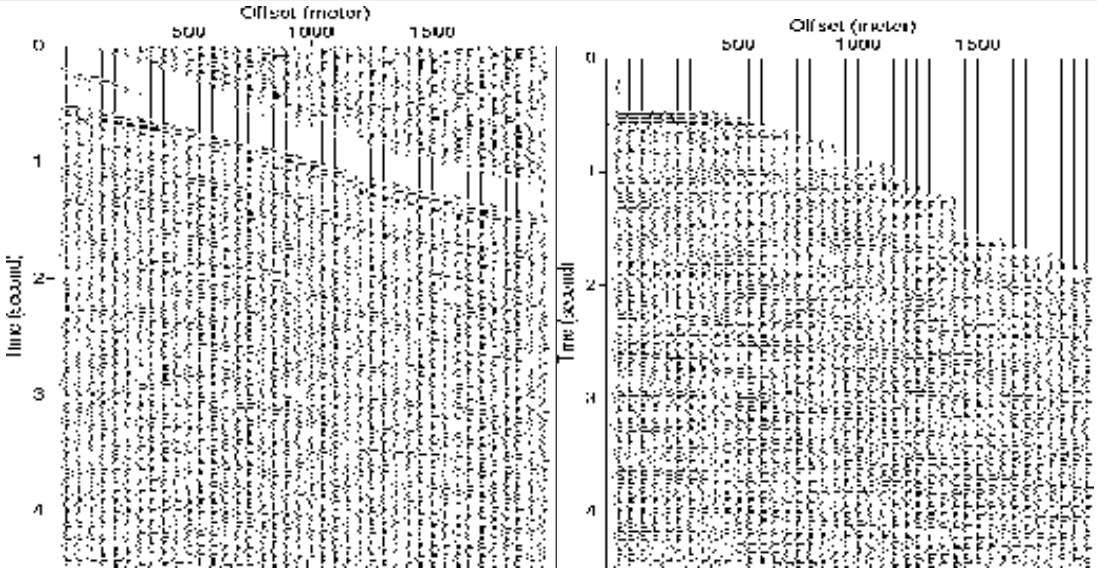

7- Velocity Analysis to Determine Vstack.

Figure 1.17 illustrates the procedure for automatically determining the stacking/NMO velocities from the CMG. Here, CMG amplitudes are summed together along different hyperbolas described by the traveltime equation 1.6. The summation is carried out for different values of ($t0$, V_{NMO}), and the result is contoured in ($t0$,V_{NMO}) space (see the RHS of Figure 1.17). The correct values of ($t0$, V_{NMO}) will describe an hyperbola that coincides with the reflection event to give a large summation value; otherwise the summation values (or semblance) are small. The summation value is called a semblance value because we really sum over a thick hyperbolic line, weight the summation with a normalization factor, and insure positive summation values by taking the absolute value of the sum.

Identifying the bullseyes on the RHS of this figure, and connecting lines between these bullseyes describes the optimal v_{NMO} vs $t0$curve. The v_{NMO} can also be thought of as the stacking velocity for a layered medium, and is considered to be good estimate of v_{RMS}.

Figure 1.17: CMG panel and corresponding semblance panel. There are 2 groups of reflection events, one corresponding to reflections from a shallow reflector with a velocity of about 5,000 ft/s, and the other from a deeper reflector with a moveout velocity of about 10,000 ft/s. Note that the bullseyes in the semblance panels correspond to the correct T0 and NMO velocities.

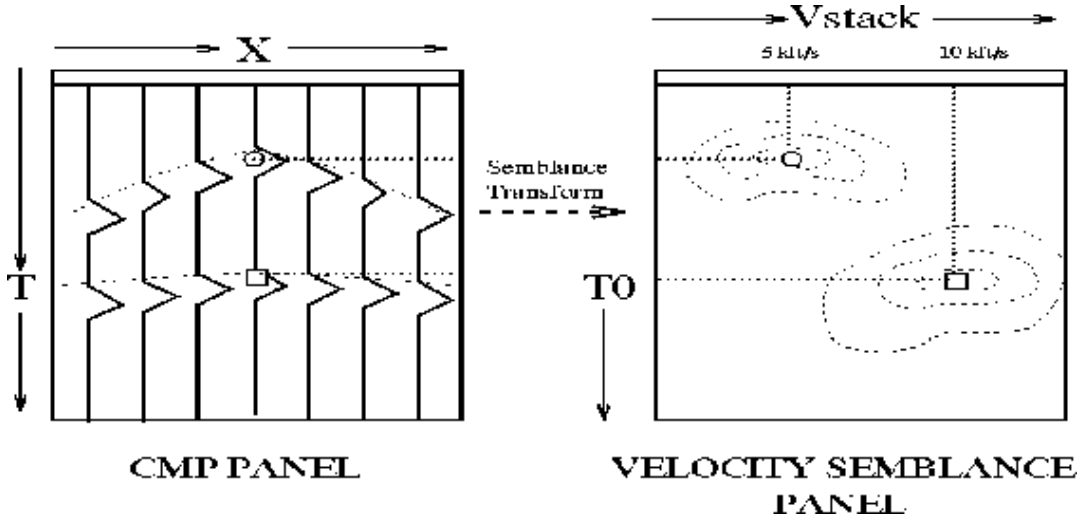

8- Stacking to Remove Coherent+Random Noise.

The NMO corrected data in a CMG are now ready to be summed together to form the stacked trace. The MATLAB code for stacking traces in a CMG is given below:

```
for x=1:nx;
for t0=1:nt;
 trace(t0) = trace(t0) + datanmo(x,t0);
end;
end;
```

One problem that arises with NMO corrected data is the phenomenon of "stretch", where the far-offset NMO-corrected traces are stretched to a wider frequency. If the stretching is too severe then you just mute such traces prior to stacking.

After stacking the traces in a CMG you get a single stacked trace of your seismic section. Placing all of the stacked traces next to one another provides you with a poststack or ZO seismic section similar to that shown in Figure 1.2. Note that using a stacking velocity tuned to the reflections allows you to reinforce the reflection energy and partly suppress the coherent noise such as surface waves, multiples, etc.. Thus, the ideal ZO section containing only primary reflections is more closely realized.

9- Poststack Migration to Go from Data Space to Model Space.

Zero-offset seismic traces (x,z=0,t)do not provide an accurate picture of the subsurface layers when there is a great deal of structural complexity. For example, Figure 1.18 shows that the apparent reflection point deduced from our traces does not coincide with the actual reflection point in which the reflection energy originated.

Figure 1.18: For a dipping layer, projecting reflection energy directly to a depth of *vt* below a trace defines the apparent reflection point, which is not the same as the actual reflection point. Thus the stacked section $d(x,z=0,t)$ is not a good approximation to $m(x,z)$for complex structures or layers with steep dip. Here *t* is the 1-way reflection time.

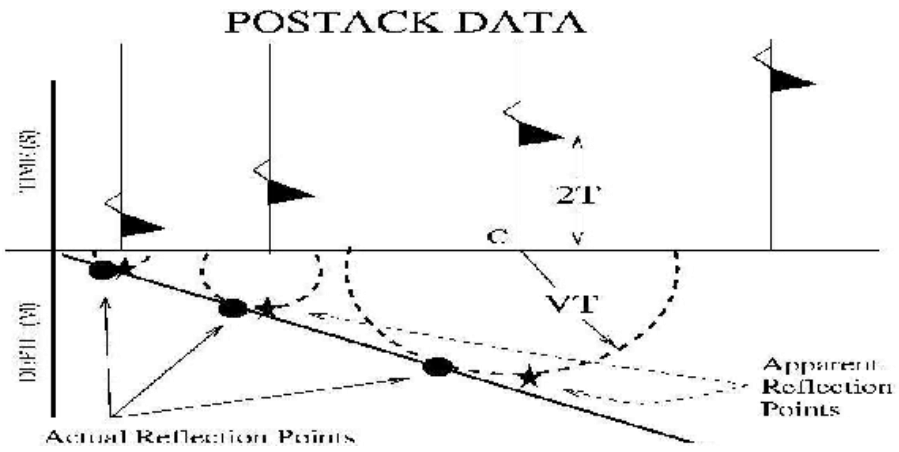

The inability of $d(x,z=0,t)$ to represent the seismic section gets even worse when your reflector becomes more complex as shown in Figure 1.19. For example, the faults in the data have diffraction tails which are collapsed in the migrated section. To correct for these distortions we apply the operation of migration to the zero-offset seismic data to produce an image $m(x,z)$ of the reflectivity section in (x,z).

Formally, if $\mathbf{L}$ is the forward modeling operator so that

$$\mathbf{d} = \mathbf{Lm}, \tag{1.11}$$

then migration can be described as the first iterate of a steepest descent method:

$$\mathbf{m} = [\mathbf{L^T L}]^{-1}\mathbf{L^T d}, \qquad \cong \mathbf{L^T d}. \tag{1.12}$$

The migration algorithm will be explained in detail by other speakers. In fact, migration of the prestack data (i.e., CMP traces) is now commonly used today to improve the imaging quality even more.

Question: Why is $\mathbf{L^T}$ such a good approximation to L^{-1}?

Answer: If the data $\mathbf{d} = \mathbf{Lm}$ roughly resemble *m*, then this suggests that $\mathbf{L}$ acts almost like an identity operator in mapping model space to data space. Thus, $\mathbf{L^T}$ might act like an inverse operator. Also, $[\mathbf{L^T L}]$ is somewhat diagonally dominant so that its inverse can be roughly approximated by a weighted diagonal matrix.

Figure 1.19: (Top) Poststack migrated image and (bottom) stacked seismic section. Note how the faults are more clearly delineated and the diffraction frowns are collapsed in the migrated section. Data are computed for the SEG/EAGE synthetic overthrust model.

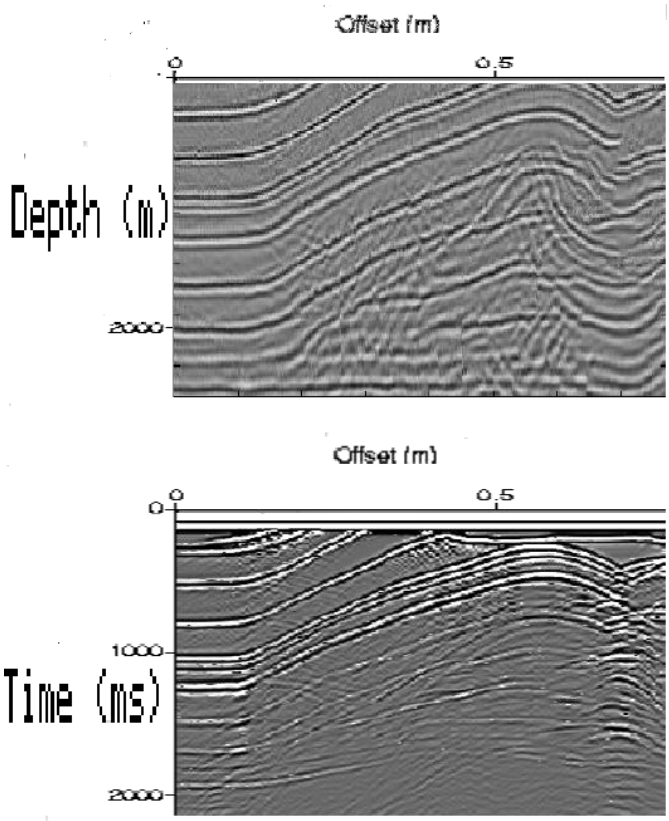

Summary

The goal of exploration seismologists is to obtain the reflectivity model of the earth. This is partly achieved by collecting non-zero offset seismic data in the format of CSG's, reorganizing them into CMG's, filtering these data, applying static and NMO time shifts to correct these data to the ZO time, and stacking to get the poststack seismic section. The stacking process is the most powerful step in eliminating both coherent and random noise. For this reason and to also increase spatial resolution, offset traces with source-receiver offsets out to more than several miles are not uncommon and sections with more than 100 fold are also used. To get an even better approximation to $m(x,z)$ the migration operator $L^T d$ is applied to these data.

Assumptions implicit in the data processing include:

- Data are largely governed by the acoustic isotropic wave equation, where density variations are weak.
- Primary reflections only in the stacked section. This means that the processing has largely eliminated coherent noise such as multiples, converted PS reflections, surface waves, etc..
- Velocity distribution is known in order to properly migrate data. Velocity semblance analysis usually does a pretty good job for geology that is not too complex.
- No reflection events originate from out-of-the-recording plane are in the data. Otherwise 3-D data should be collected and processed in a 3-D fashion.

References

Yilmaz, O., 1987, Seismic Data Processing: SEG Publishing, Tulsa, Ok.